Optimised Parameter Sets for Thermographic Inspection of CFRP Metal Hybrid Components

Michael Jelinek, Johannes Schilp, Gunther Reinhart

CIRPe 2015 - Understanding the life cycle implications of manufacturing

Optimised Parameter Sets for Thermographic Inspection of CFRP Metal Hybrid Components

Michael Jelinek[a,*], Johannes Schilp[a], Gunther Reinhart[b]

[a]Institute for Machine Tools and Industrial Managemenet – Application Centre Augsburg, Beim Glaspalast 5, D-86153 Augsburg, Germany
[b]Institute for Machine Tools and Industrial Management, Boltzmannstraße 15, D-85748 Garching, Germany

*Corresponding author. Tel.: +49-821-56883-56; fax: +49-821-56883-50. E-mail address: Michael.Jelinek@iwb.tum.de

Abstract

The current development trend in automotive engineering as well as in aviation features an increased substitution of metal components by carbon fibre reinforced plastic (CFRP) structures. However, material-specific requirements make a complete replacement of a metal construction by CFRP structures impracticable. Consequently, metallic regions remain in the CFRP base body as metal joints or reinforcements. Frequently, these hybrid transition areas are involved with an increased quality concern. This research explores the methodological deduction of test specimens which allow an thermographic investigation of typical defects based on predefined industrial CFRP machine elements concretely (shaft coupling, hollow shaft, gripper arm). Thereby, the optimisation through systematic parameter variation and the structured parameter documentation in a database are focused within the present research. By deriving inspection task-specific user guidelines, the predominantly manual thermographic testing process can be considerably accelerated.

1. Introduction

The thermographic referencing process of carbon fibre reinforced plastic (CFRP) structures in order to ascertain optimal thermographic testing parameters for the subsequent documentation of the obtained parameter sets in a structured database constitutes the scope of the present paper.

Preceding studies specify material-specific characteristics of CFRP metal hybrid compounds as well as the thermographic testing parameters exerting considerable influence on the failure contrast (signal-noise ratio – SNR) [1]. Defective test specimens referring to the material-specific parameters are inspected via variation of the relevant thermographic testing parameters for the purpose of achieving the maximal SNR as well as the optimal SNR in relation to the associated measurement time. Thereby, the attention is directed to special structures as a CFRP gripper arm.

1.1. Thermographic inspection of CFRP metal compounds

The inspection of CFRP metal hybrid components utilising active thermography is gradually intensified. Especially safety-related structures in the aerospace [2], automotive and energy industry are analysed assigning active thermography as a non-destructive evaluation (NDE) technique [3]. Nevertheless, a standardised inspection procedure depending on the actual thermographic testing exercise is currently non-existent [3].

Active thermography is capable of being employed during [4] and after the manufacturing process as well as concerning in-service testing in particular [5, 6, 7]. [1] declares typical stages extracted from a CFRP component lifecycle in which the application of NDE by active thermography is feasible.

The signal-noise ratio (SNR) [8] arising from the thermographic inspection solely characterises the visibility of

an imperfection. In particular, the modulation of the excitation frequency exerts remarkable influence on the obtainable SNR [1]. The signal-noise ratio (SNR) defines a failure contrast with reference to [9] and [10].

$$SNR = \frac{|M_{high} - \overline{M}_d| + |M_{low} - \overline{M}_d|}{|M_{high,Ref} - \overline{M}_{Ref}| + |M_{low,Ref} - \overline{M}_{Ref}|} \quad (1)$$

M_{high} and M_{low} represent average phase angle values in a damaged area (objective: **phase contrast**) while $M_{high,Ref}$ and $M_{low,Ref}$ characterise average phase angle values in a defect-free area of the CFRP structure (objective: **reference contrast**). $\overline{M}_d$ expresses the global average value of the phase angle in a defective and $\overline{M}_{Ref}$ in a defect-free area of a region of interest (ROI) [1]. In this context, a ROI is defined as distinctly combined CFRP laminate materials paired with an optional metal joint or reinforcement. This material mix can include one specific failure such as delamination, fibre crack, or porosity [1].

The conceptualised thermographic referencing procedure in regard to a ROI of a CFRP metal hybrid structure is presented in [1] (Figure 1). Further information concerning active thermography as well as NDE is provided in [11-14].
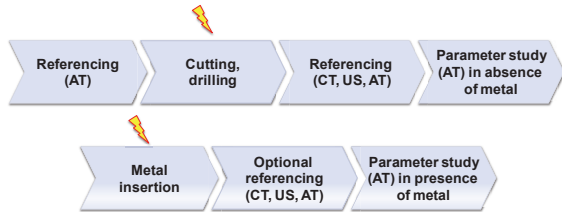

Fig. 1. Stadiums in a complete referencing process of a CFRP metal hybrid test specimen. A potentially defective CFRP structure is marked with a bolt symbol with reference to [1].

1.2. Thermographic inspection of CFRP in the presence of metallic joints or reinforcements

A major problem related to the thermographic inspection of CFRP structures comprises the thermal zone of influence resulting in a glowing effect, and consequently, in a decrease of failure contrast adjacent to a metallic joint or reinforcement [1, 15, 16] (Figure 11).

The main objective lies on the determination of optimal parameter sets compromising over the minimal thermal glowing and the achievable SNR.

2. Deduction and examination of defined defective test specimens regarding the gripper arm (structural element)

2.1. Identification of heavily loaded structural areas with the assistance of the finite element method (FEM)

The deduction of defined defective test specimens in dependence on the structural element is based on the finite element method (FEM). The FEM provides information about the inference regions, prognosticates the heavily loaded zones of the structure resulting from utilisation, and the expected potential defects [17]. Figure 2 demonstrates the load simulation applying the FEM on the structural element.

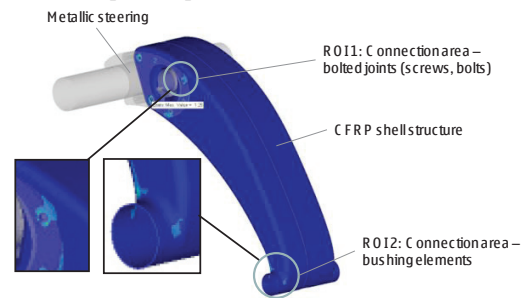Certain heavily loaded areas (ROI) to be focused on in a non-destructive inspection process are declared.

Fig. 2. FEM analysis of the gripper arm (structural element) and declaration of heavily loaded areas (max. static deformation: 1.72) in utilisation.

2.2. Deduction of defined defective test specimens in reference to the FEM

In terms of particular imperfections in the connection area of metal and CFRP, plate-shaped test specimens containing defined delaminations (polytetrafluoroethylene – PTFE slides) and fibre cracks (dissected fibres) adjacent to bolted joints were manufactured with reference to [1] and [18]. Furthermore, plate-shaped test specimens relevant to the connection area of bushings comprise delaminations, fibre cracks and debonding. Structures in a different shape as tubular specimens regarding bushings include artificial delaminations. The manufacturing process is described by the complete construction of the specimen, subsequently by the lamination process and finally by cutting and drilling as well as by the integration of the metal components (screws, bolts, bushings) in the CFRP base body (Figure 3).
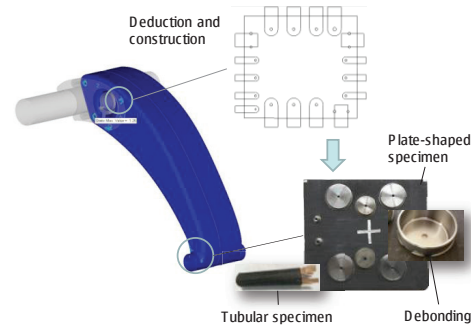

Fig. 3. Deduction, construction and building of defined defective test specimens resulting from heavily loaded areas of the machine element.

The specimens were all manufactured containing the same symmetric lay-up composed of eight layers Prepreg (Table 1).

Table 1. Basic lay-up of all test specimens in correspondence to the original industrial machine element.

Layer no.	Material	Designation	Orientation
1	woven fabric	CE 8201 KDK E201	±45°
2	unidirectional	CE 1250-230-39 E201	0°
3	woven fabric	CE 8201 KDK E201	±45°
4	woven fabric	CE 8201 KDK E201	0°/90°
	Symmetric lay-up		

The adhesive employed to integrate metal joints was Araldite 2015 Huntsman two component epoxy resin. The bushings with a diameter of 50 mm, 38 mm, 24 mm and 10 mm were made of stainless steel (1.4104.05). The screws were placed into rivet nuts (RIVKLE with SKG, sizes M5, M6, M8) that were directly embedded into the CFRP base body of the specimens. Further bolted joints were realised by Cherry Maxibolt elements (CR7620S-06-03, 5 mm).

2.3. Thermographic referencing procedure of test specimens

The thermographic equipment employed for the complete investigation at *iwb* Application Centre Augsburg consists of the following components:

Table 2. Thermographic testing equipment applied for the investigation of test specimens at *iwb* Application Centre Augsburg.

Excitation	Source	Description
Optical	Halogen spots	Hedler (2x H25s lamps per spot, 1250 W per lamp) and reflector "Hedler MaxiSun"
Optical	Flash light	Hensel VH3-6000 Linear Head (max. flash energy: 6000 J)
Eddy current	Inductor	IFF IS-0352 (coil length: 100 mm, coil width: 28 mm)
Thermographic camera (IR camera)	FLIR SC5000	FLIR SC5650, cooled photo quanta detector, resolution: 640 x 512 pixel, sensitivity: 20 mK, temperature range: -20°C to +3000 °C, weight: 3.8 kg, maximum image refresh rate: 380 Hz
Thermography system	edevis®	OTVis, PTVis, ThermoVis, image evaluation software: DisplayIMG 6

The plate-shaped specimens resembling the fibre cracks contained cuts through the rovings (lengths: 3 mm, 5 mm, 10 mm) in certain layers (1, 2, 3, 4 relevant to the connection area of bushings; 1, 3, 5, 7 relating to the connection area of bolted joints). The test specimens were examined by eddy current (30 kHz, Inductor: IFF IS-0352) before drilling and integrating metal elements into the CFRP.

Table 3. Results of eddy current method by plate-shaped CFRP specimens containing fibre cracks in certain layers. Testing set-up: transmission, distance to surface of the inductor: 5 mm, excitation frequency: 30 kHz, lateral offset of the inductor to the ROI: 150 mm.

Fibre crack	3 mm	5 mm	10 mm
Layer 1	+	+	+
Layer 2	o	+	+
Layer 3	o	o	+
Layer 4	ND	o	o
Layer 5	ND	ND	o
Layer 6	ND	ND	ND
Layer 7	ND	ND	ND
Layer 8	ND	ND	ND
Detectability: + good, o insecure, ND not detectable			

Subsequent to the fibre crack referencing, the holes were drilled in CFRP structure with taking the actual positions of the artificial defects into account. By causing fibre cuts, drilling leads to the interruption of the current flow in the CFRP structure beginning from the lateral width of the hole and extending to its periphery along the fibre orientation in a certain layer. Drilling holes causes that merely the defects positioned exteriorly are still detectable. The reachable detection depth remains constant (Table 3).

The integration of the metal elements like bushings, rivet nuts or bolts results in a decreased failure contrast. The detection of fibre cracks is solely possible in a certain distance from the metal element (about 10 mm) while the detection depth remains the same as shown in Table 3.

The imperfections caused by debonding (defined lack of adhesive) are non-detectable employing the existent examination methods (optical - halogen, optical - flash, eddy current). These imperfections between the metal element and the CFRP base body were constituted solely of adhesive gaps extending to a maximum of 2 mm. The gap angle circulating the metal element (38 mm diameter) reached the magnitude 180°. The delamination sizes and depths in the plate-shaped test specimens as well as in the tubular specimens are summarised in Table 4. To ensure validity, each failure was placed not less than three times in the test specimens, which additionally could be examined on the reverse.

Table 4. Artificially integrated delaminations in plate-shaped and tubular test specimens, insertion and removal of PTFE slides after curing.

Delaminations in plate-shaped specimens (x existent, - not existent)						
Delamination located beneath	15x25 mm	25x25 mm	30x30 mm	40x25 mm	70x40 mm	90x40 mm
Layer 1	-	x	-	x	x	x
Layer 2	x	x	x	x	x	x
Layer 3	-	x	-	x	x	x
Layer 4	x	x	x	x	x	x
Layer 5	-	x	-	x	x	x
Layer 6	x	x	x	x	x	x
Layer 7	-	x	-	x	x	x

Delaminations in tubular specimens (x existent, - not existent)				
Delamination located beneath	3x6 mm	5x10 mm	7x14 mm	10x20 mm
Layer 1	x	x	x	x
Layer 2	-	-	-	-
Layer 3	-	-	-	-
Layer 4	x	x	x	x
Layer 5	-	-	-	-
Layer 6	-	-	-	-
Layer 7	x	x	x	x

The initial stadium of the referencing process is characterised by investigating the existence of the artificially integrated imperfections as well as by the specification of the drilling positions in relation to the existent defects. The holes were positioned either on the delaminated area or precisely on

the defect margin. Figure 4 presents the thermogram of a referenced plate-shaped specimen possessing delaminations as well as the specified drilling positions.

The positions 3, 4, 7, 8, 12 and 13 are highly suitable for the methodological deduction of the optimal, thermographic testing parameters to achieve a maximum failure contrast adjacent to a metallic joint.
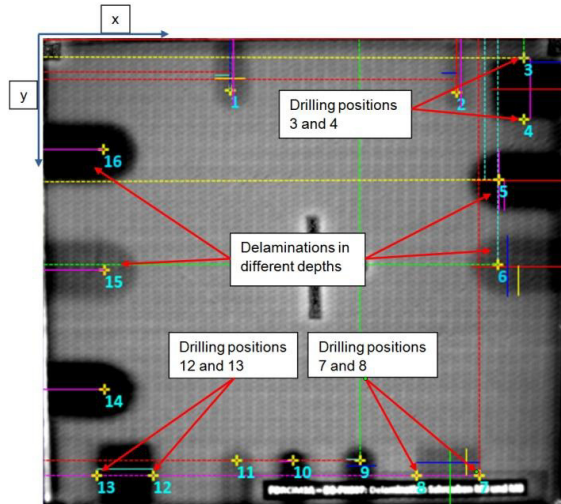

Fig. 4. Referencing defined imperfections of different sizes and depths employing active thermography (lock-in frequency: 0.01 Hz, halogen excitation, testing set-up: reflection).

2.4. Further referencing with applying additional testing methods to ascertain the absence of additional damages resulting from drilling and cutting operations

To ensure the non-existence of further damages caused by the drilling process, the plate-shaped test specimens were completely referenced by computer tomography (CT) and the ultrasound technique (US). By utilising these independent methods, the precise position and size of the artificially integrated delaminations could be verified.

2.5. Thermographic parameter study in the absence of metal joints or reinforcements

Following the second referencing stadium, the optimal thermographic testing parameter set is methodologically identified. In order to achieve this objective, the following approach was developed.

Despite the fact that the examination should theoretically be realised in absence of a metal element, there is also the possibility to execute it in the presence of a metal component. However, this operation demands the non-existence of thermal interference between the metal part and the CFRP area to be evaluated. As the maximum failure contrast (SNR) is substantially affected by the lock-in frequency, this parameter was varied stepwise (1 Hz, 0.7 Hz, 0.5 Hz, 0.3 Hz, 0.1 Hz, 0.07 Hz, 0.05 Hz, 0.03 Hz, 0.01 Hz, 0.005 Hz). On the contrary, the number of measuring periods (MP) does not exert noticeable influence on the SNR [1]. Therefore, a constant value of 3 MP to record phase images was used.

The evaluation of the picture data was performed applying the Software DisplayIMG 6 (edevis®). Particular failure zones and intact areas were declared exploiting certain overlays (lines, squares) in the thermograms. The software exports the values of the phase angle pixel by pixel in dependence on the complexity of the overlay geometry, either along the line or within the limits. Figure 5 depicts the exportation of the pixel values relying on the phase angle along "failure lines" (F) and "reference lines" (R).
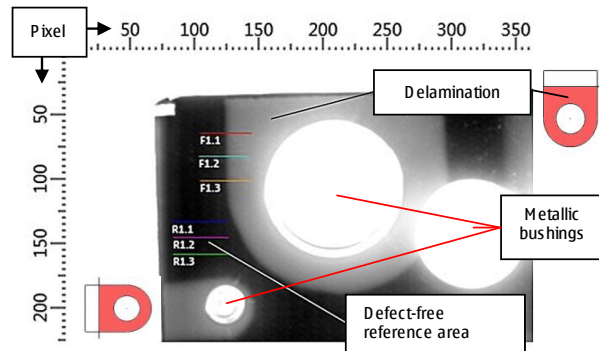

Fig. 5. Referencing defined imperfections of different sizes and depths applying active thermography (lock-in, frequency: 0.03 Hz, halogen excitation, testing set-up: reflection).

The phase angle along the lines as well as the **differences** between failure- and corresponding reference lines are demonstrated pixel by pixel (Figure 6 and 7). Alternatively, the mentioned lines can be extracted from rectangular overlays. This approach protocols the phase shift from an intact area to a defective zone in the CFRP structure (pixel 17-23).
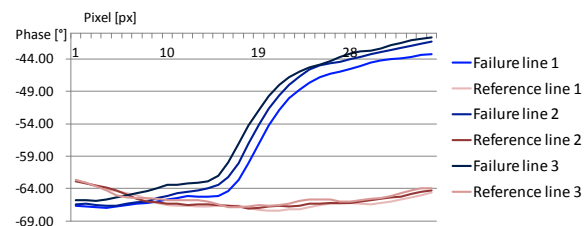

Fig. 6. Analysis of a thermogram created with one specific parameter set employing failure and reference lines.
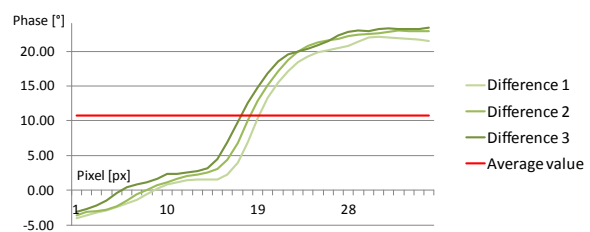

Fig. 7. Differences between failure and corresponding reference lines.

In the final step of the parameter study, the **phase contrast** is determined by subtracting the averaged phase angle values deviating negatively and positively from a global average phase value (red line in Figure 7 and 8, see Formula 1).
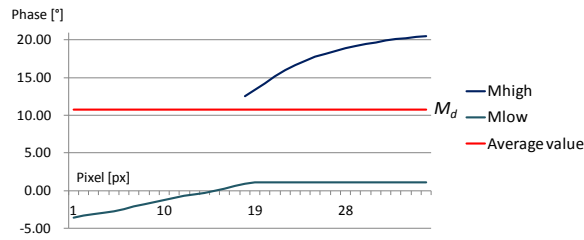
Fig. 8. Determining of a phase contrast based on failure and reference lines (Figure 6) in reference to Formula 1.

The SNR results from dividing the phase contrast values by a **reference contrast**, equivalent to a noise value (Formula 1), which can be determined in the same way as the phase contrast. Therefore, all overlay lines (failure and reference lines) are located in a defect-free area of the thermogram. In the analysis of the SNR obtained through variation of Fourier frequency (lock-in frequency), one or more maxima can be recognised (Figure 9). The accomplished studies lead to values of a barely visible thermographic failure contrast of "1.2" resulting from Formula 1.
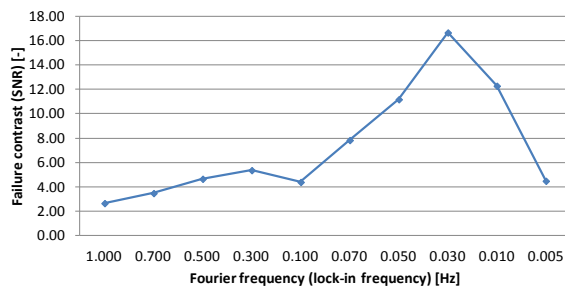

Fig. 9. Documentation of the failure contrast (SNR) varying the Fourier frequency (lock-in frequency) of the thermographic excitation.

The measurement time to create a thermogram involves the evaluation of both the present parameter set and the resultant SNR values above 1.2. These values are divided by their corresponding measurement time in seconds. The resulting curve is shown by Figure 10.
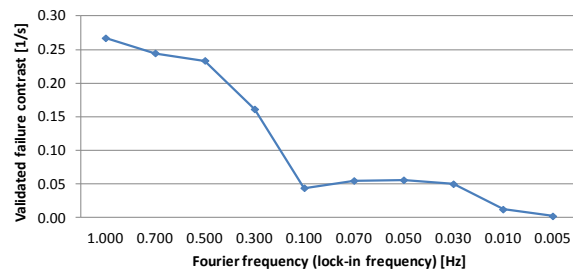

Fig. 10. Documentation of the failure contrast (SNR) varying the Fourier frequency (lock-in frequency) of the thermographic excitation, evaluated by dividing the values by the corresponding measurement time in seconds.

The above-mentioned evaluation of the SNR leads to the conclusion that the documentation of two frequency values (maximum of SNR, optimal SNR in relation to the associated measurement time) in a structured parameter database concerning the optimal thermographic testing parameters emerges as reasonable.

The results obtained from the inspection of both the plate-shaped and the tubular test specimens by means of optical thermography (lock-in, impulse) are documented in Table 5.

In general, the failure depth and the bending of the CFRP material exert direct influence on the Fourier frequency leading to an optimal failure contrast. On the contrary, the failure size solely plays a subordinate role in the determination of the Fourier frequency.

Independent of the structural geometry, the flash excitation is feasible up to layer 4 whereby an intensified lateral thermal conduction by curved structures slightly reduces the depth of heat penetration (detection uncertainty at layer 4).

Table 5. Results from the examination of both the plate-shaped and the tubular test specimens by optical thermography. First value: lock-in frequency (Hz) leading to a maximum of SNR, second value: lock-in frequency (Hz) leading to the optimal SNR corresponding to measurement time. "Flash", if impulse thermography led to a visible SNR.

Delaminations in plate-shaped specimens (- not existent)						
Delamination located beneath	15x25 mm	25x25 mm	30x30 mm	40x25 mm	70x40 mm	90x40 mm
Layer 1	-	0.01 0.5 Flash	-	0.01 0.5 Flash	0.03 0.1 Flash	0.03 0.7 Flash
Layer 2	0.3 0.3 Flash	0.01 0.3 Flash	0.01 0.3 Flash	0.01 0.3 Flash	0.01 0.3 Flash	0.01 0.3 Flash
Layer 3	-	0.01 0.3 Flash	-	0.01 0.3 Flash	0.01 0.5 Flash	0.01 0.1 Flash
Layer 4	0.005 0.05 Flash	0.005 0.05 Flash	0.03 0.3 Flash	0.005 1.0 Flash	0.01 0.5 Flash	0.005 0.3 Flash
Layer 5	-	0.01 0.1	-	0.01 0.1	0.005 0.3	0.01 0.1
Layer 6	0.01 0.1	0.01 0.1	0.01 0.1	0.005 0.5	0.005 0.03	0.07 0.1
Layer 7	-	0.005 0.005	-	0.005 0.07	0.01 0.03	0.01 0.01

Delaminations in tubular specimens (- not existent, ND not detectable)				
Delamination located beneath	3x6 mm	5x10 mm	7x14 mm	10x20 mm
Layer 1	0.5 1.0 Flash	0.5 1.0 Flash	0.5 1.0 Flash	0.5 1.0 Flash
Layer 2	-	-	-	-
Layer 3	-	-	-	-
Layer 4	ND	0.1 0.1	0.1 0.1 Flash	0.1 0.1 Flash
Layer 5	-	-	-	-
Layer 6	-	-	-	-
Layer 7	ND	ND	0.07 0.07	0.07 0.07

2.6. Thermographic parameter study in the presence of metallic joints or reinforcements

The final stadium describes the determination of the optimal excitation frequency resulting in both a maximum of failure contrast (SNR) and the optimal SNR in correlation to the associated measurement time, adjacent to metallic elements like bushings or bolted joints. The issue of a thermal interference zone leading to a glowing effect, and consequently, to a decrease of SNR contiguous to the metallic element in the CFRP base body is clarified by Figure 11 showing the behaviour of a plate-shaped CFRP test specimen equipped with bushings.
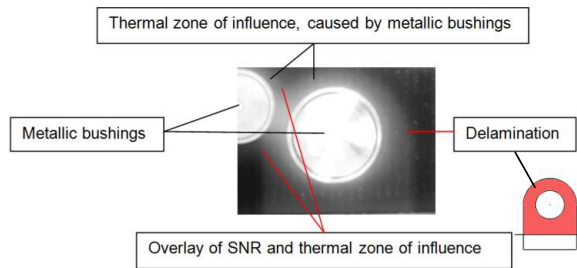

Fig. 11. Glowing effect and the consequent decrease of SNR adjacent to bushings in a plate-shaped CFRP base body.

The method to determine the required Fourier frequencies corresponds to the procedure already discussed, except the fact that evaluation of the SNR is to be performed in certain distances (px) from the margin of the metal component. Apart from the exploitation of conventional failure and reference lines, the possibility to extract phase angle values alternatively from rectangular overlays in the thermogram exists. It is obligatory, that the failure lines are completely embedded into the thermal interference zone caused by the metallic element. By this means, errors occurring in the phase contrast specification are precluded. Figure 12 illustrates one possible orientation of failure and reference lines by examining of a delamination adjacent to a metallic bushing.
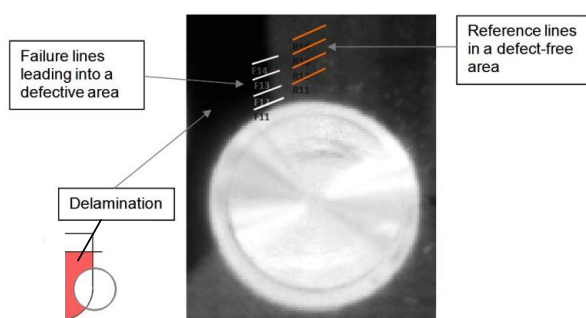

Fig. 12. Position and orientation of four failure and four reference lines (failure lines: white, reference lines: orange) to examine a delamination adjacent to a metallic bushing in a plate-shaped CFRP base body.

Determining the optimal Fourier frequencies to achieve a maximum of SNR and the optimal SNR in correlation to the associated measurement time involves the generation of a **phase contrast** with subtracting the phase angle values along the failure and reference lines. Adjacent to metallic elements, the obtained differences vary depending on the distance of the failure lines to the margin of the metal element. In the analysis, four failure lines were exemplarily located in certain distances from a metallic bushing (1 px, 5 px, 10 px, 15 px). Figure 13 and 14 depict a decreasing SNR contiguous to the metallic element (the curve resulting from a distance of 1 px is not declining as intensively as the curve corresponding to a distance of 5, 10 or 15 px respectively).
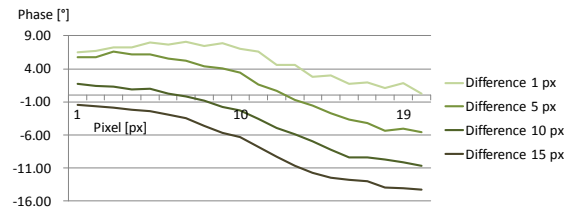

Fig. 13. Differences of failure and reference lines in certain distances (1 px, 5 px, 10 px, 15 px) from a metallic element in the CFRP base body.
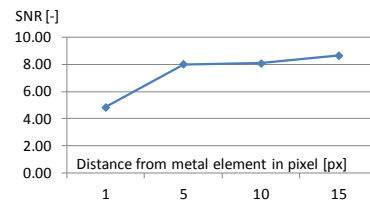

Fig. 14. Decreasing SNR contiguous to the metallic element (1 px, 5 px, 10 px, 15 px) in the CFRP base body.

The interpretation of a CFRP metal hybrid ROI with varying Fourier frequency results in certain frequencies receiving a maximum of SNR yet close to the metal element (Figure 15). Inconsistencies as well as measuring errors can effectively be excluded from the evaluation by setting all SNR values lower than "1.2" to "zero" as well as zeroing the SNR, if the SNR neighbouring the metallic element possesses a greater value than the SNR in major distance.
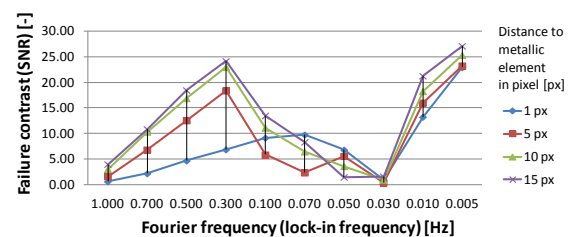

Fig. 15. SNR in certain distances (1 px, 5 px, 10 px, 15 px) from a metallic element in a CFRP base body.

The final evaluation via division of the SNR by the associated measurement time in seconds is presented in Figure 16.
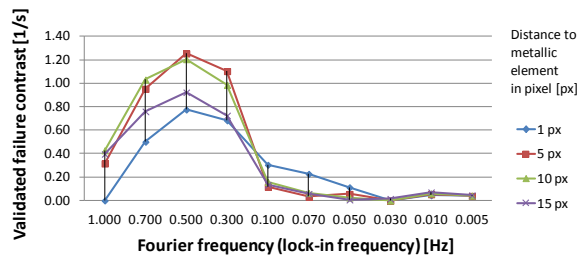
Fig. 16. SNR in certain distances (1 px, 5 px, 10 px, 15 px) from a metallic element in a CFRP base body evaluated in dependence on the measurement time.

Despite the fact that the above-mentioned method has already been fully developed, it has to be validated by the application on further CFRP metal hybrid test specimens. The results of the validation process as well as additional, optimal thermographic parameter sets, which can be integrated into a structured database, are expected as outcome from the prospective research project. Concerning this matter, first steps have already been pursued regarding a CFRP coupling and a CFRP hollow shaft.

3. Summary and prospect

The present paper exhibits the capability of deducing defined defective test specimens based on industrial CFRP metal hybrid components. The usage of the FEM allows the characterisation of highly stressed zones and the corresponding defects in the inspected components.

The inferred information enables the assembly of artificially defective specimens. The variation of relevant thermographic testing parameters – particularly the Fourier frequency – in order to obtain the optimal parameter sets constitutes a remarkable section of the referencing procedure which represents the fundamental step to standardise the thermographic inspection process. In this context, an optimal parameter set is characterised either by the maximal failure contrast or by the optimal failure contrast regarding a preferably short measurement time.

The optimal parameter sets ultimately acquired through the thermographic investigation of defined defective test specimens – especially adjacent to metallic joints – are intended to be documented in a structural database, which has already been basically developed.

The systematic storage together with the subsequent provision of the optimal testing parameters enables the enhanced execution of the thermographic inspection procedure and customisation for the user-requirements. Via realising the knowledge management in the form of a database, the thermographic testing process is optimised.

4. Acknowledgement

References

[1] Jelinek M, Seidel C, Reinhart G. Thermographic Inspection of CFRP Metal Hybrid Structures. CIRPe2015. Cranfield (UK): Elsevier 2015.

[2] Ibarra-Castanedo C, Grinzato E, Marinetti S, Bison P, Genest M, Grenier M, Piau JM, Benada A, Maldague X. Recent progresses in the inspection of aerospace components by infrared thermography. 17th World Conference on Nondestructive Testing. Shanghai: 2008.

[3] Maierhofer C, Myrach P, Steinfurth H, Reischel M, Röllig M. Development of standards for flash thermography and lock-in thermography. 14th International Conference on Quantitative InfraRed Thermography (QIRT14). University of Bordeaux, Bordeaux: 2014.

[4] Ullmann T, Schmidt T, Hofmann S, Jemmali R. In-line Quality Assurance for the Manufacturing of Carbon Fiber Reinforced Aircraft Structures. 2nd International Symposium on NDT in Aerospace 2010 – Tu.1.A.4. Hamburg: 2010.

[5] Ibrahim ME. Nondestructive evaluation of thick-section composites and sandwich structures: A review. Composites: Part A 64 (2014). Fishermans Bend: Elsevier 2014. p. 35-48.

[6] Zöcke CM. Quantitative analysis of defects in composite material by means of optical lockin thermography. Dissertation. Naturwissen-schaftliche Technische Fakultät III Chemie, Pharmazie, Bio- und Werkstoffwissenschaften, University of Saarland and Ecole Doctorale MIM of Université Paul-Varlaine / Metz. Saarbrücken and Metz: 2009.

[7] Wu D, Busse G. Lock-in thermography for nondestructive evaluation of materials. Rev. Gén. Therm. (1998) 37. Paris: Elsevier 1998. p. 693-703.

[8] Madruga FJ, Albenda P, Ibarra-Castanedo C, López-Higuera JM. Signal to noise ratio (SNR) comparison for lock-in thermographic data processing methods in CFRP specimen. 10th International Converence on Quantitative InfraRed Thermography (QIRT10). Québec: 2010.

[9] Balageas DL, Chapuis B, Deban G, Passily F. Quantitative assessment of the improvement of the detection of defects by pulse thermography thanks to the TSR approach in the case of a smart composite repair patch. 10th International Conference on Quantitative InfraRed Thermography. Québec: 2010.

[10] Maldague XPV, Largouet Y, Couturier J-P. A study of defect depth using neural networks in pulsed phase thermography: modelling, noise, experiments. Rev. Gén. Therm. (1998) 37. Paris: Elsevier 1998.

[11] Meola C. Infrared Thermography Recent Advances and Future Trends. Bentham eBooks 2012.

[12] Holst GC. Common Sense Approach to Thermal Imaging. WA: SPIE Optical Engineering Press. Bellingham: 2000.

[13] Maldague XPV. Theory and Practice of Infrared Technology for Non Destructive Testing. New York: Wiley 2001.

[14] Siemer U. Einsatz der Thermografie als zerstörungsfreies Prüfverfahren in der Automobilindustrie – Entwicklung einer Ingenieurplattform. Dissertation. Naturwissenschaftlich Technische Fakultät III Chemie, Pharmazie und Werkstoffwissenschaften. University of Saarland. Saarbrücken: 2010.

[15] Wilhelm M, Füssel U, Nancke T, Duschl M. Herausforderung CFK-Stahl-Mischbau: Quantifizierung von Delaminationen infolge des umformtechnischen Fügens. DGZfP-Jahrestagung 2013 – Mi.3.C.1. DGZfP 2013.

[16] Aderhold J, Meinlschmidt P. Grundlagen der Online-Thermographie (article 2). In: Bauer N. Leitfaden zur Wärmefluss-Thermographie – Zerstörungsfreie Prüfung mit Bildverarbeitung. Fraunhofer-Gesellschaft zur Förderung der angewandten Forschung e.V. Erlangen: 2005. p. 5-7. ISBN: 3-8167-6754-0.

[17] Oster R. Non-destructive testing methodologies on helicopter fiber composite components challenges today and in the future. 18th World Conference on Nondestructive Testing, Durban: 2012.

[18] Reischel M, Myrach P, Maierhofer C. Development of Reference Test CFRP Specimens for Standardisation of Active Thermography with Flash Excitation. 4th International Symposium on NDT in Aerospace 2012 – Th.4.A.1. Augsburg: 2012.